Extension of Analytical Indicial Aerodynamics to Generic Trapezoidal Wings in Subsonic Flow

Andrea Da Ronch*, Daniel Kharlamov† and Antonino Ventura‡

Faculty of Engineering and the Environment

University of Southampton, Southampton, SO17 1BJ, U.K.

Marcello Righi§

School of Engineering, Zurich University of Applied Sciences

8401, Winterthur, Switzerland

Matteo Franciolini¶

Dipartimento di Ingegneria Industriale e Scienze Matematiche

Università Politecnica delle Marche, I-60100 Ancona

Marco Berci‖

School of Mechanical Engineering

University of Leeds, LS2 9JT, Leeds, UK

Analytical indicial aerodynamic functions are calculated for a number of trapezoidal wings in subsonic flow, with Mach number $0.3 \leq M \leq 0.7$. The formulation herein proposed extends well–known aerodynamic theories, which are limited to thin aerofoils in incompressible flow, to generic trapezoidal wing planforms. First, a thorough study is executed to assess the accuracy and limitation of analytical predictions, using unsteady results

*Lecturer, AIAA Senior Member and Atmospheric Flight Mechanics Technical Committee Member. Correspondence: A.Da-Ronch@soton.ac.uk; Tel.: +44-23-8059-4787.

†PhD student.

‡Visiting MSc student, Politecnico of Turin, Italy.

§Professor, AIAA Member.

¶PhD student.

‖Visiting Academic, AIAA Member.

from two state–of–the–art computational fluid dynamics solvers as cross–validated benchmark. Indicial functions are calculated for a step change in angle of attack and for a sharp–edge gust, each for four wing configurations and three Mach numbers. Then, analytical and computational indicial responses are used to predict dynamic derivatives and the maximum lift coefficient following the encounter with a one–minus–cosine gust. It is found that the analytical results are in excellent agreement with the computational results for all test cases. In particular, the deviation of the analytical results from the computational results is within the scatter or uncertainty in the data arising from using two computational fluid dynamics solvers. This indicates the usefulness of the developed analytical theories.

Keywords: Indicial aerodynamics; Analytical approach; Computational fluid dynamics; Compressible flow; Angle of attack response; Gust response

Nomenclature

c	Wing chord
C_L	Wing lift coefficient due to a unit step–change in angle of attack
$\breve{C}_L$	Wing circulatory lift coefficient due to a unit step–change in angle of attack
$\hat{C}_L$	Wing non–circulatory lift coefficient due to a unit step–change in angle of attack
k	Reduced frequency
M	Mach number
m_α	Number of terms in the approximation of the non-circulatory lift due to a step–change in angle of attack
m_G	Number of terms in the approximation of the non-circulatory lift due to a sharp–edge gust
n_α	Number of terms in the approximation of the circulatory lift due to a step–change in angle of attack
n_G	Number of terms in the approximation of the circulatory lift due to a sharp–edge gust
Re	Reynolds number
t	Physical time
U_∞	Freestream speed

Greek

α_0	Freestream angle of attack
$\delta\alpha$	Amplitude of angle of attack change
Δ_0	Distance of the first cell off the wing surface
λ	Wing taper ratio

Λ Wing sweep angle

τ Nondimensional time

τ_0 Nondimensional delay for gust encounter

I. Introduction

Indicial theory is a powerful mathematical tool that has been extensively employed in aerodynamics modelling (refer to Ref.[1] and references therein). Indicial theory asserts that the response of a linear time invariant system to an arbitrary input can be constructed by integrating a linear functional which involves the knowledge of the time dependent input signal and a kernel response. The kernel is an inherent characteristic of the system. Adding a nonlinear dependence of the functional on the input level[2] extends the capability of the model, allowing a certain class of model nonlinearity to enter the response. It is also important to observe that the traditional Volterra–Wiener theory[3,4] of nonlinear systems represents a subset of nonlinear indicial theory.

Researchers have followed three paths to address the indicial aerodynamic modelling: an analytical path, a numerical path using high–fidelity computational fluid dynamics (CFD) techniques, and an experimental path using measurements obtained in wind tunnel dynamic tests.

Analytical theories were derived under the assumption of thin aerofoil in incompressible, irrotational and two–dimensional flow. In the 1920s, Wagner[5] conducted a series of studies for the unsteady lift generated on an aerofoil due to abrupt changes in angle of attack. The Wagner function describes the indicial built–up of the circulatory part of the lift, including the influence of the shed wake. Theodorsen[6] extended those studies investigating the forces and moments on an oscillating aerofoil. The lift response of an aerofoil penetrating sharp–edge and harmonically varying gusts were studied by Küssner[7] and Sears,[8] respectively. Further details on analytical theories of indicial aerodynamics and some recent developments, including the approach herein proposed, are given in Section II.

Advances in computational power have allowed significant progress in the use of CFD techniques for modelling of nonlinear unsteady aerodynamics. To overcome the limitations of analytical indicial aerodynamics, restricted to linear flows and thin aerofoils, researchers investigated a number of alternatives. The first attempts to directly determine the indicial response by CFD date back to 1990s.[9] This approach has received widespread use (see Refs.[10,11] among many others) but still presents a number of difficulties, mostly associated with the numerical settings of the analysis and the reliability of the unsteady results.

Other researchers have approached the modelling problem using indicial aerodynamics

derived from wind tunnel dynamic tests and flight test measurements. For example, Refs.[12,13] applied linear indicial models to data from different testing facilities and different aircraft models. The identification of indicial models from flight test data were documented in Ref.[14] Nonlinear indicial responses were applied to the rolling 65 deg delta wing,[15] and in Ref.[16] to the prediction of a dynamically stalling wing.

A substantial portion of the work described in this paragraph was motivated by the increased manoeuvre capabilities and expanded flight envelope of modern aircraft. More recently, under the NASA Aviation Safety Program, further research in unsteady modelling has been carried out at NASA Langley Research Center, and an excellent review of these methodologies is presented in Ref.[1]

The main contribution of this work is the derivation of an analytical indicial aerodynamics method that extends well–known theories, which are based on the assumption of thin aerofoils, to generic trapezoidal wings of finite span in subsonic flow. In particular, the paper is built around three objectives. The first is the formulation, application and demonstration of a consistent analytical framework for predicting the unsteady aerodynamic responses to arbitrary changes in the angle of attack and in the vertical component of the freestream speed (gusts). The second objective places emphasis on the use of current state–of–the–art CFD modelling techniques, as provided by a widely–available open source solver as well as an industrial grade solver, for predicting unsteady viscous flows. The third objective draws a final assessment of the analytical model predictions in light of the CFD–based unsteady aerodynamics uncertainty. A set of trapezoidal wings, with different aspect ratio (AR) and sweep angle, are tested at different flow conditions. In total, 24 unsteady aerodynamic test cases are executed for each methodology.

The paper continues in Section II with the analytical derivation of indicial aerodynamic functions valid for generic trapezoidal wings in subsonic flow. Section III summarises the computational solvers and the appropriate techniques for the calculation of indicial aerodynamics. Then, results for four wing configurations and a set of flow conditions are presented and discussed in Section IV, highlighting the computational advantages and the related limitations where appropriate. Finally, conclusions are drawn in Section V.

II. Analytical Derivation of Indicial Functions

Building on previous work,[17] aerodynamic indicial functions for compressible subsonic flows are herein approximated by modification of the indicial functions for an incompressible flow. Prandtl–Glauert scalability[18] is used for the circulatory contribution, $\breve{C}_L(\tau)$, and piston theory[19] for the non–circulatory contribution, $\hat{C}_L(\tau)$. The lift coefficient is then found using the principle of superposition, $C_L = \breve{C}_L + \hat{C}_L$.

The analytical formulae are derived combining the work of Queijo[20] with that of Leishman.[21] The former describes the wing circulatory lift in incompressible flow, including the wake two–dimensional downwash and the tip vortices three–dimensional downwash.[22] The latter provides a theory for the calculation of thin aerofoil lift in compressible flow, including Prandtl–Glauert theory for the circulatory terms and piston theory for the non–circulatory terms.

The circulatory lift build–up due to a unit sharp–edge gust with perturbation front parallel to the wing leading edge is then calculated multiplying the lift response to a step change in angle of attack with the ratio between Küssner and Wagner functions.[23] It is worth observing that the latter represents a fictitious angle of attack[24] and approximates the two–dimensional penetration effect within the "frozen gust" framework.[25]

The non–circulatory contribution drives the impulsive–like start of the flow response for any wing shape and is followed by a short yet complex region where outgoing and incoming acoustic waves intersect.[19] The circulatory contribution drives the subsequent lift build–up until steady state convergence. As the asymptotic lift value provided by Queijo[20] is originally deemed inaccurate, it is here obtained via simplified lifting–line theory.[26] An alternative for fine–tuning the asymptotic value is to use available numerical or experimental data,[27] so that viscous effects may statically be recovered in the absence of significant flow separation[28]. With identical reference flow conditions, the initial lift coincides for both tuned and untuned cases but later develops with a different rate.

For swept wings, the entry delay relative to each section is geometrically known and considered when obtaining the lift build–up due to a unit sharp–edge gust with perturbation front normal to the reference airflow.

A. Circulatory Part

Considering a trapezoidal flat wing with aspect ratio AR, taper ratio λ and sweep angle Λ, a simplified yet effective parametric model was formulated to calculate the lift build–up due to a unit step in the angle of attack for incompressible flow.[20]

Denoting $M_e = M\cos(\Lambda)$ the effective Mach number and $\beta = \sqrt{1 - M_e^2}$ the Prandtl–Glauert compressibility factor, the original analytical model may be extended to compressible subsonic flow in the absence of shock waves, as the (linear) scaling laws break down in the (nonlinear) transonic regime[29]. The asymptotic steady–state lift coefficient due to a step change in angle of attack is formulated as:[18]

$$\bar{C}_L = \frac{2\pi\, AR\cos(\Lambda)}{2\,(1+\delta)\cos(\Lambda) + AR\,\beta} \tag{1}$$

where δ is the wing efficiency factor that can be calculated via lifting–line theory[26] for a

straight wing in incompressible flow, or more generally used as fine–tuning parameter.

The circulatory component of the lift due to a step change in the angle of attack is written as:

$$\breve{C}_L^{\alpha} = \bar{C}_L \left(1 - \breve{k} \sum_{j=1}^{n_\alpha} \breve{A}_j^{\alpha} \, e^{-\breve{B}_j^{\alpha} \, \beta^2 \, \tau} \right), \qquad \sum_{j=1}^{n_\alpha} \breve{A}_j^{\alpha} = 1 - \frac{\breve{C}_L^*}{\bar{C}_L^*}, \qquad \breve{k} = \frac{\bar{C}_L^*}{\bar{C}_L} \left(\frac{\bar{C}_L - \breve{C}_L}{\bar{C}_L^* - \breve{C}_L^*} \right) \tag{2}$$

where $\breve{C}_L^*$ and $\bar{C}_L^*$ are the initial and final values of the circulatory lift coefficient as provided by Queijo[20] (see the Appendix), whereas $\breve{C}_L = \breve{C}_L^*/E$ is the actual initial value with E the complete elliptic integral of the second kind;[22] the n_α coefficients $\breve{A}_j^{\alpha}$ and $\breve{B}_j^{\alpha}$ are obtained by best–fitting the entire indicial function for incompressible flow.

For the gust encounter, it is assumed that the "frozen gust" approach[23] is valid and that the gust front is parallel to the wing leading edge. The circulatory lift development due to a sharp–edged gust is written as:

$$\breve{C}_L^{G} = \bar{C}_L \left(1 - \sum_{j=1}^{n_G} \breve{A}_j^{G} \, e^{-\breve{B}_j^{G} \, \beta^2 \, \tau} \right), \qquad \sum_{j=1}^{n_G} \breve{A}_j^{G} = 1 \tag{3}$$

where the n_G coefficients $\breve{A}_j^{G}$ and $\breve{B}_j^{G}$ are obtained by best–fitting the indicial lift resulting from multiplying the circulatory lift development due to a unit step in the angle of attack by the ratio between Küssner's and Wagner's functions for the case of incompressible flow (see the Appendix), thus accounting for the gust–entry delay.[30]

For the four wing configurations of this study (see Figure 1), Table 1 reports the optimal coefficients for approximating the indicial lift function to a step change in angle of attack in incompressible flow with $n_\alpha = 3$, while Table 2 reports those to approximate the response to a sharp–edge gust with $n_G = 4$. All coefficients were obtained via constrained nonlinear optimisation[31] by minimising the root–mean–square error between the approximate and original curves in the Appendix.

Table 1. Optimal coefficients for approximating the indicial lift function to a step change in angle of attack in incompressible flow

AR	Λ [deg]	$\breve{A}_1^{\alpha}$	$\breve{A}_2^{\alpha}$	$\breve{A}_3^{\alpha}$	$\breve{B}_1^{\alpha}$	$\breve{B}_2^{\alpha}$	$\breve{B}_3^{\alpha}$
8	0	0.0521	0.2407	0.1452	0.0482	0.1896	0.5963
8	30	0.0276	0.1099	0.0865	0.0485	0.2137	0.7722
20	0	0.0872	0.2362	0.1516	0.0401	0.1618	0.5612
20	30	0.0374	0.1111	0.0908	0.0400	0.1933	0.7400

Table 2. Optimal coefficients for approximating the indicial lift function to a sharp–edge gust in incompressible flow

AR	Λ [deg]	$\breve{A}_1^G$	$\breve{A}_2^G$	$\breve{A}_3^G$	$\breve{A}_4^G$	$\breve{B}_1^G$	$\breve{B}_2^G$	$\breve{B}_3^G$	$\breve{B}_4^G$
8	0	0.1038	0.4189	0.3124	0.1648	0.0687	0.2787	1.2485	15.964
8	30	0.0913	0.4004	0.3508	0.1575	0.0635	0.2830	1.1679	16.194
20	0	0.1184	0.3773	0.3341	0.1702	0.0486	0.2158	0.9424	12.320
20	30	0.0969	0.3747	0.3732	0.1553	0.0472	0.2352	0.9712	13.838

B. Non–circulatory Part

The exact non–circulatory lift contribution is analytically known via piston theory and extends into a complex transitory region where the indicial function presents a change of slope,[32] which originates from an interaction between outgoing and incoming acoustic waves leaving the aerofoil at $\hat{\tau} = 2M_e/(1 + M_e)$ and $\breve{\tau} = 2M_e/(1 - M_e)$, respectively. For $\tau \leq \hat{\tau}$, the initial behaviour is:[19]

$$C_L^\alpha = \frac{4}{M}\left[1 - \left(\frac{1 - M_e}{2M_e}\right)\tau\right], \qquad C_L^G = \frac{2\cos(\Lambda)}{\sqrt{M_e}}\,\tau \tag{4}$$

The non–circulatory lift contributions may then be approximated with a series of damped oscillatory terms[17] as:

$$\hat{C}_L^\alpha = \sum_{j=1}^{m_\alpha} \hat{A}_j^\alpha\, e^{-\hat{B}_j^\alpha\,\beta^2\,\tau}\,\cos\left(\hat{\Omega}_j^\alpha\,\beta^2\,\tau\right), \qquad \hat{C}_L^G = \sum_{j=1}^{m_G} \hat{A}_j^G\, e^{-\hat{B}_j^G\,\beta^2\,\tau}\,\cos\left(\hat{\Omega}_j^G\,\beta^2\,\tau\right) \tag{5}$$

where the coefficients $\hat{A}$, $\hat{B}$ and $\hat{\Omega}$ may be obtained by best–fitting the difference between (exact) piston theory and (approximate) circulatory contribution, subject to the nonlinear constrains:

$$\sum_{j=1}^{m_\alpha} \hat{A}_j^\alpha = \frac{4}{M} - \check{C}_L, \qquad \sum_{j=1}^{m_\alpha} \hat{A}_j^\alpha\,\hat{B}_j^\alpha = \bar{C}_L\,\breve{k}\sum_{j=1}^{n_\alpha} \breve{A}_j^\alpha\,\breve{B}_j^\alpha + 2\,\frac{(1 - M_e)}{M\,M_e\,\beta^2} \tag{6}$$

$$\sum_{j=1}^{m_G} \hat{A}_j^G = 0, \qquad \sum_{j=1}^{m_G} \hat{A}_j^G\,\hat{B}_j^G = \bar{C}_L\sum_{j=1}^{n_G} \breve{A}_j^G\,\breve{B}_j^G - 2\,\frac{\cos(\Lambda)}{\sqrt{M_e}\,\beta^2} \tag{7}$$

which satisfy the exact initial behaviour of piston theory up to first–order accuracy.

For practical applications,[21] a single exponential term (i.e., $m_\alpha = 1$ with $\hat{\Omega}_1^\alpha = 0$) is

often employed for the case of a unit step in the angle of attack, namely:

$$\hat{A}_1^\alpha = \frac{4}{M} - \breve{C}_L, \qquad \hat{B}_1^\alpha = \frac{1}{\hat{A}_1^\alpha}\left[\bar{C}_L\,\breve{k}\sum_{j=1}^{n_\alpha}\breve{A}_j^\alpha\,\breve{B}_j^\alpha + 2\,\frac{(1-M_e)}{M\,M_e\,\beta^2}\right] \tag{8}$$

whereas at least two exponential terms (i.e., $m_G = 2$ with $\hat{\Omega}_1^G = 0$ and $\hat{\Omega}_2^G = 0$) are necessary for the case of a unit sharp–edged gust, namely:

$$\hat{A}_1^G = -\,\bar{C}_L\,\breve{A}_{n_G}^G, \qquad \hat{B}_1^G = \frac{1}{\hat{A}_1^G}\left(\bar{C}_L\sum_{j=1}^{n_G-1}\breve{A}_j^G\,\breve{B}_j^G - \frac{2\cos(\Lambda)}{\sqrt{M_e}\,\beta^2}\right) \tag{9}$$

along with $\hat{A}_2^G = \bar{C}_L\,\breve{A}_{n_G}^G$ and $\hat{B}_2^G = \breve{B}_{n_G}^G$ to cancel the initial behaviour of the circulatory contribution.

In fact, this simple arrangement departs quite soon from the correct behaviour,[17] whereas retaining the trigonometric term and letting the approximation pass through the last point given by piston theory at $\tau = \hat{\tau}$ lead to higher–order accuracy, with:

$$\hat{\Omega}_1^\alpha = \frac{\arccos}{\beta^2\hat{\tau}}\left\{\frac{e^{\hat{B}_1^\alpha\beta^2\hat{\tau}}}{\hat{A}_1^\alpha}\left[\frac{8M_e}{M\,(1+M_e)} - \bar{C}_L\left(1-\breve{k}\sum_{j=1}^{n_\alpha}\breve{A}_j^\alpha e^{-\breve{B}_j^\alpha\beta^2\hat{\tau}}\right)\right]\right\} \tag{10}$$

$$\hat{\Omega}_1^G = \frac{\arccos}{\beta^2\hat{\tau}}\left\{\frac{e^{\hat{B}_1^G\beta^2\hat{\tau}}}{\hat{A}_1^G}\left[\frac{4\cos(\Lambda)\sqrt{M_e}}{1+M_e} - \bar{C}_L\left(1-\sum_{j=1}^{n_G-1}\breve{A}_j^G e^{-\breve{B}_j^G\beta^2\hat{\tau}}\right)\right]\right\} \tag{11}$$

C. Normal Front Gust

When the front of the sharp–edge gust is normal to the reference airflow, each wing section of a swept wing encounters the gust front at a different time. This effect mitigates the initial lift build–up and shall be taken into account. The entry delay relative to a wing section at the spanwise location y is geometrically known as $\tau_0 = 2\tan(\Lambda)\,y/c$. Therefore, in the special case of a rectangular wing, the circulatory contribution becomes:

$$\breve{C}_L^G = \begin{cases} \bar{C}_L\left[\frac{\tau}{AR\tan(\Lambda)} - \sum_{j=1}^{n_G}\frac{\breve{A}_j^G}{\breve{B}_j^G}\left(\frac{1-e^{-\breve{B}_j^G\beta^2\tau}}{\beta^2\,AR\tan(\Lambda)}\right)\right], & 0 < \tau < AR\tan(\Lambda) \\ \bar{C}_L\left[1 - \sum_{j=1}^{n_G}\frac{\breve{A}_j^G}{\breve{B}_j^G}\left(\frac{e^{\breve{B}_j^G\beta^2\,AR\tan(\Lambda)}-1}{\beta^2\,AR\tan(\Lambda)}\right)e^{-\breve{B}_j^G\beta^2\tau}\right], & \tau > AR\tan(\Lambda) \end{cases} \tag{12}$$

whereas, using a single yet effective exponential term, the non–circulatory contribution reads:

$$\hat{C}_L^G = \begin{cases} \sum_{j=1}^{m_G} \frac{\hat{A}_j^G}{\hat{B}_j^G} \left(\frac{1 - e^{-\hat{B}_j^G \beta^2 \tau}}{\beta^2 \, AR \tan(\Lambda)} \right), & 0 < \tau < AR \tan(\Lambda) \\ \sum_{j=1}^{m_G} \frac{\hat{A}_j^G}{\hat{B}_j^G} \left(\frac{e^{\hat{B}_j^G \beta^2 \, AR \tan(\Lambda)} - 1}{\beta^2 \, AR \tan(\Lambda)} \right) e^{-\hat{B}_j^G \beta^2 \tau}, & \tau > AR \tan(\Lambda) \end{cases} \tag{13}$$

III. Numerical Calculation of Indicial Functions

Two CFD solvers are used to benchmark analytical predictions. The first is the `DLR-Tau` code, which is widely employed in the European aerospace industry, and the second is `SU2`, an open–source code.

A. Computational Fluid Dynamics Solvers

The `DLR-Tau` code [a] is a finite volume unstructured method which solves the Reynolds–averaged Navier–Stokes equations on a cell–vertex metrics. The code is used to solve both steady and unsteady problems, and both dual time stepping and global time stepping are supported for the latter. Explicit and implicit solution algorithms have been implemented, based on Runge–Kutta methods for explicit calculations and a LU–SGS method for implicit calculations. The inviscid flux terms can be treated with either central, upwind or hybrid schemes. Either matrix or scalar dissipation is used to stabilise the convective central difference operators. Viscous terms are treated using a conventional central differencing scheme. The calculations presented in this work were obtained using the dual time stepping approach of Jameson.[33] The convergence rate was improved with a full multi–grid W–cycle acceleration technique based on agglomerated coarse grids. The original version of the Spalart–Allmaras (SA) model is used for the turbulence closure.

The `SU2` software suite[34–36] is an open–source collection of software tools written in C++ and Python for performing multi–physics simulation and design. It is built specifically for the analysis of partial differential equations (PDEs) and PDE–constrained optimization problems on unstructured meshes with state–of–the–art numerical methods, and it is particularly well suited for aerodynamic shape design. The initial applications of the suite were mostly in aerodynamics, but through the initiative of users and developers around the world, `SU2` is now being used for a wide variety of problems beyond aeronautics, including automotive, naval, and renewable energy applications, to name a few. In all calculations presented, convective fluxes are modelled according to Roe's scheme[37] with the Venkatakrishnan limiter.[38] The standard dual time stepping was used in all cases. The Krylov problem was solved with FGMRES method and the LU–SGS preconditioner. No multi–grid acceleration was used.

[a] http://tau.dlr.de/startseite/

The original version of the SA model has been used also for SU2.

B. Unsteady Motions

The calculation of indicial responses is carried out for two unsteady motions. One motion corresponds to a step change in angle of attack, with amplitude $\Delta\alpha = 1.0$ deg. The second motion is for a sharp–edge gust with the vertical component of the velocity, normalised by the freestream speed U_∞, equal to $w_g \approx 0.0174$ (approximating the ratio $\pi/180$). For both cases, the background steady–state flow solution was calculated at a freestream angle of attack $\alpha_0 = 0.0$ deg.

In the DLR-Tau solver, the unsteady motions are performed via a rigid grid–movement approach. Adopting physical time, t, a generic translation, $\chi(t)$, is formulated as:

$$\chi = \sum_{k=0}^{N_{PT}} p_k\, t^k + a_0 + \sum_{k=0}^{N_{FT}} \left(a_k \cos(k\,\omega_T\, t) + b_k \sin(k\,\omega_T\, t)\right) \tag{14}$$

Similarly, a generic rotation, $\phi(t)$, is expressed by:

$$\phi = \sum_{k=0}^{N_{PR}} r_k\, t^k + c_0 + \sum_{k=0}^{N_{FR}} \left(c_k \cos(k\,\omega_R\, t) + b_k \sin(k\,\omega_R\, t)\right) \tag{15}$$

The terms N_{PT} and N_{PR} denote, respectively, the number of polynomial coefficients used to model the translation and rotation. The terms N_{FT} and N_{FR} denote, respectively, the number of Fourier coefficients. In this work, the step change in angle of attack was forced imposing a constant velocity in the vertical direction ($N_{PT} = 1$, $p_1 = U_\infty \arctan(\Delta\alpha)$).

In SU2, the step change in the angle of attack is also realised by imposing a constant vertical velocity as a rigid body motion.

The gust analysis in DLR-Tau is performed using a grid–velocity approach.[9] This method modifies the flux balance in the computational domain by an additional disturbance field representative of the prescribed gust. The disturbance is prescribed in the initial field, typically the steady–state solution, and is allowed to move in time depending on the shape and the position of the gust. The user can specify the shape of the gust, as function of the x–coordinate for frontal gusts, y–coordinate for lateral gusts gust and time t, selecting the global shape between the one–minus–cosine or the sharp–edge gust. The gust spatial wavelength and the velocity relative to the frame of reference can also be prescribed as input parameters.

The gust analysis in SU2 follows a different approach: the gust profile is introduced as a perturbation of the initial velocity flowfield. The sharp–edge gust front is positioned several hundred chords upstream of the wing leading edge. The perturbation is extended upstream

indefinitely, and is propagated towards the wing at the freestream speed.

IV. Results

Four configurations of trapezoidal wings are considered. The geometric parameters include the wing sweep angle, $\Lambda = 0$ and 30 deg, and the aspect ratio, $AR = 8$ and 20. The baseline aerofoil, taken parallel to the flow direction, is based on the NACA 0006 aerofoil which is extruded in the span–wise direction. The wing tip is sharp in all cases, and the corresponding cross–section is parallel to the incoming flow. A schematic of the four wing configurations is shown in Figure 1. Note that the aspect ratio is given for the tip–to–tip wing geometry, according to the usual convention used in the analytical formulation. For each configuration, the indicial lift response is computed for three Mach numbers (0.3, 0.5 and 0.7) for a step change in angle of attack and for a sharp–edge gust. The Reynolds number, based on the chord, is set to $11.7 \cdot 10^6$ for the $M = 0.7$ case, and reduced accordingly for the lower speed cases. In total, 24 test cases (four geometric configurations, three Mach numbers and two responses) involving unsteady simulations are performed.

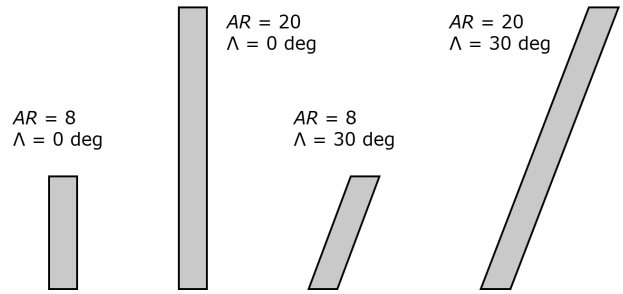

Figure 1. A schematic of the four wing configurations

A. Spatial and Temporal Convergence

Unstructured grids were generated with `Pointwise`®, and `T-Rex` was used to create a regular boundary layer off the wing surface. The grid topology contains a far–field boundary condition that is set, on average, at 100 times from the wing surface. Symmetry boundary conditions are set on the vertical plane of symmetry, and the boundary conditions at the wing surface are modelled as adiabatic wall.

To begin with, tests were performed on a set of three grids to ensure results presented are independent from the spatial discretisation. The refinement of the grids was done by increasing systematically the nodes of all connectors by 30%, while the initial wall distance was maintained constant at $\Delta_0 = 1 \times 10^{-6}$. The spatial convergence check was performed for the $AR = 20$, $\Lambda = 0$ deg wing at $M = 0.7$. The steady state lift coefficient computed

using DLR-Tau for the three grids of this convergence study are summarised in Table 3. The term N_p indicates the number of grid points. The percentual error is calculated using Richardson's extrapolation. For the coarse grid, the DLR-Tau results achieve a percentual error smaller than 1%. The grid convergence study was also repeated for SU2, with similar considerations than those already drawn. SU2 predicts $C_L = 0.1049$ for the coarse grid, which is less than 0.4% of the value from the DLR-Tau solver. This grid was then used in the remainder of the work.

Table 3. Spatial convergence study using DLR-Tau for the $AR = 20$, $\Lambda = 0$ deg wing ($\alpha_0 = 1$ deg, $M = 0.7$)

N_p	C_L	ΔC_L [%]
$1.33 \cdot 10^6$	0.105368	0.227
$2.08 \cdot 10^6$	0.105237	0.103
$5.50 \cdot 10^6$	0.105151	0.022
Richardson	0.105128	

As computing the initial lift development requires reducing the time-step length with lowering the Mach number,[28] a second set of tests was run on the selected grid to investigate the temporal convergence of the unsteady responses. Three values of time–step size were considered: 0.025, 0.05 and 0.1 (see Figure 2(a)). Following the traditional procedure, which consists of running at least three unsteady simulations, a nondimensional time step of 0.05 was found adequate for the subsequent studies reported in this work. Furthermore, we have checked the consistency of this conclusion based on the frequency content of the indicial response to a step change in angle of attack. As an example, Figure 2(b) illustrates the amplitude of the Fourier transform for the $AR = 8$ and $\Lambda = 0$ deg wing at Mach number 0.3. The transformed signal has a limited frequency content, which decays rapidly for increasing reduced frequency. The saddle point, at $k \approx 0.5$, corresponds to the impulsive/circulatory transition of the indicial response. For $k = 10$, the frequency content decays by about 2 orders of magnitude, as expected.[39] Based on Nyquist–Shannon sampling theorem, the largest time step to resolve the indicial response for $k \in [0, 10]$ is 0.05, which is consistent with the previous consideration.

B. Indicial Response to Step Change in Angle of Attack

The indicial responses of the lift coefficient to a step change in angle of attack are shown, for all test cases, in Figures 3 and 4. Each sub–figure consists of two images. The bottom image provides the overall trend of the indicial response up to an asymptotic time, $\tau_F = 50$, while the upper image focuses on the impulsive part of the response, $0 \leq \tau \leq 4$. To facilitate cross–comparisons, the upper image also reports a schematic of the corresponding

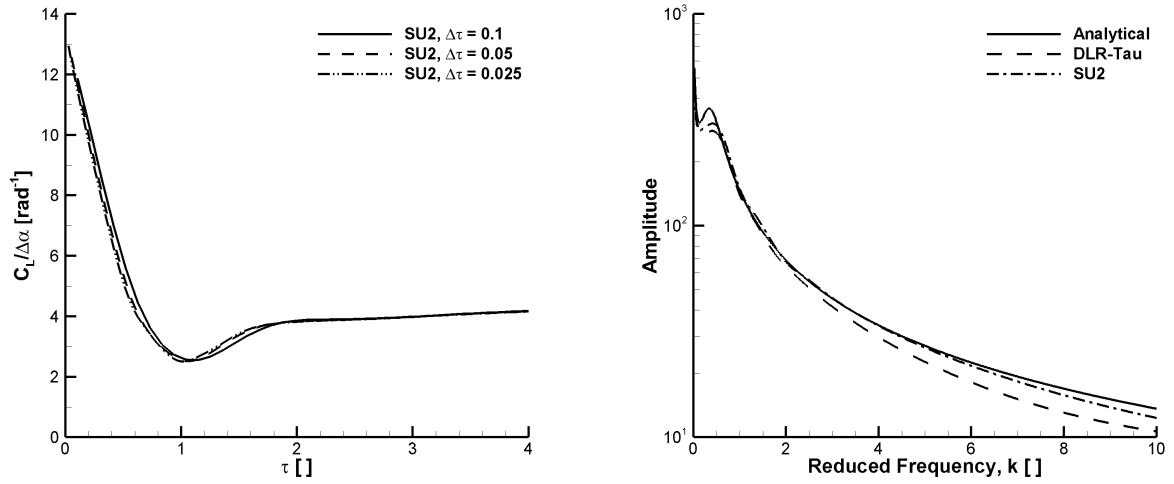

(a) $M = 0.3$, $AR = 8$, $\Lambda = 0$ deg

(b) Fourier transform with selected time step

Figure 2. In (a), indicial response to step change in angle of attack with different nondimensional time steps; in (b), Fourier transform of the indicial response with nondimensional time step of 0.05

wing configuration. In particular, Figure 3 analyses the impact of the sweep angle and Mach number for the $AR = 8$ wing, and Figure 4 for the $AR = 20$ wing. The analytical responses use $n_\alpha = 3$ and $m_\alpha = 1$ terms, respectively, for the circulatory and non–circulatory parts. Based on lifting–line theory, the wing efficiency factor is $\delta = 0.195$ for the smaller aspect ratio, and $\delta = 0.334$ for the larger one.[40]

From Figures 3 and 4, it is apparent that the initial value of the indicial response depends solely on Mach number and is independent from the wing configuration. On the other side, all sources of data are in good agreement for the asymptotic value, which is seen to decrease with the sweep angle as expected from well–known aerodynamic theories. At intermediate times, the qualitative behaviour of the indicial response is similar for different sweep angles, and the lowest value in the response is reached at a similar time. Quantitatively, the value of the lower peak depends on the wing sweep, with a smaller value for the swept–wing cases.

Differences between CFD data and analytical predictions become apparent above $M = 0.5$, particularly, for the larger aspect ratio wing. Despite some differences, the CFD data show a saddle in the indicial response at intermediate times (Figures 3(e) and 3(f), and Figures 4(e) and 4(f)), which is not modelled in the analytical function.

C. Error Quantification in Dynamic Derivatives Predictions

The impact of the observed deviations between analytical and numerical indicial responses is quantified in the context of a realistically important quantity, which is derived from the

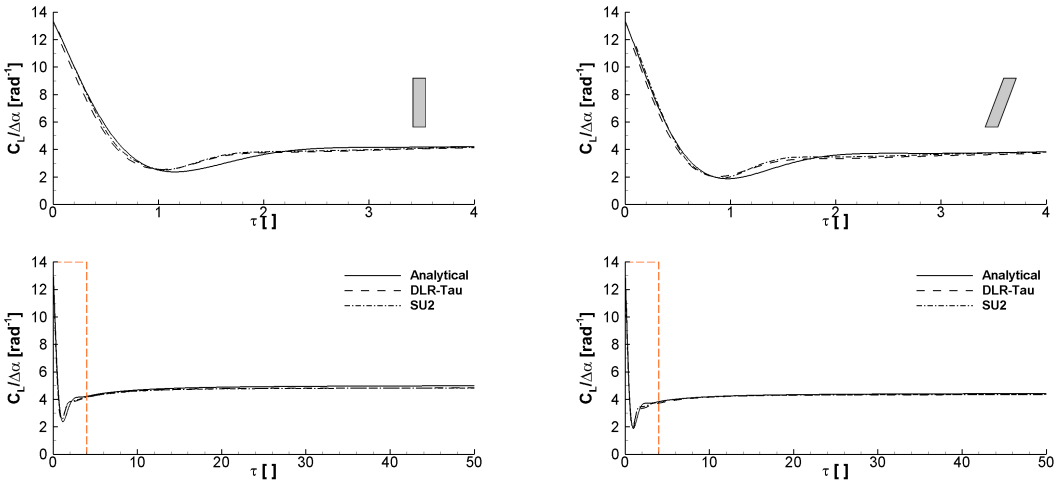

(a) $M = 0.3$, $\Lambda = 0$ deg

(b) $M = 0.3$, $\Lambda = 30$ deg

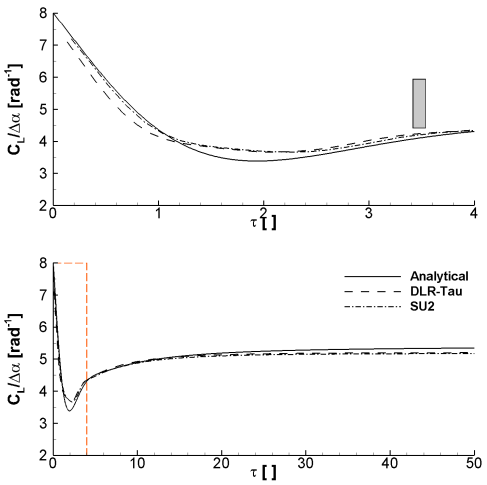

(c) $M = 0.5$, $\Lambda = 0$ deg

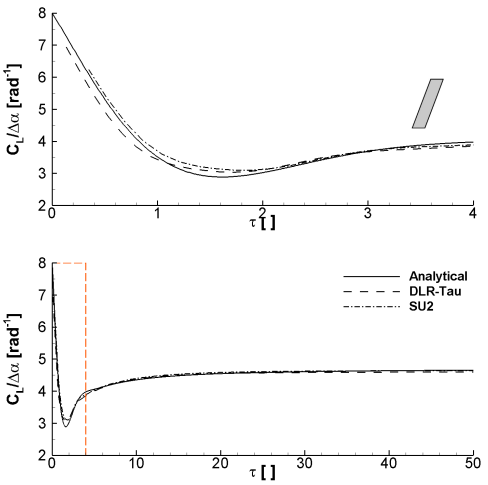

(d) $M = 0.5$, $\Lambda = 30$ deg

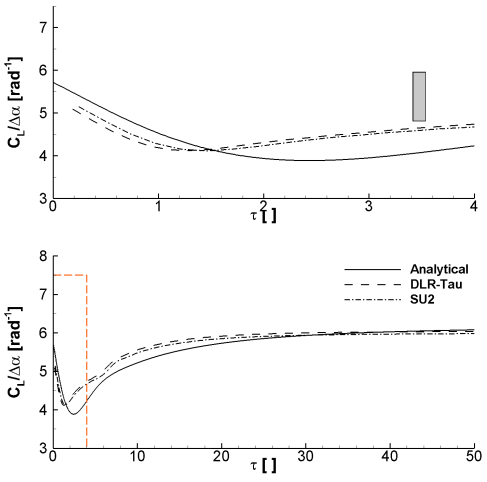

(e) $M = 0.7$, $\Lambda = 0$ deg

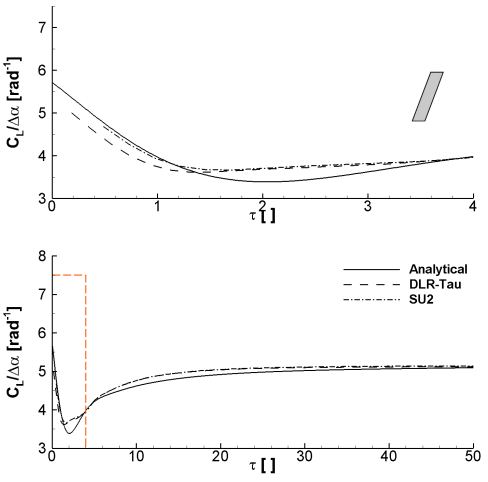

(f) $M = 0.7$, $\Lambda = 30$ deg

Figure 3. Indicial response of lift coefficient to a step change in angle of attack ($\Delta\alpha = 1.0$ deg) for the $AR = 8$ wing; figures on the left are for $\Lambda = 0$ deg, those on the right for $\Lambda = 30$ deg

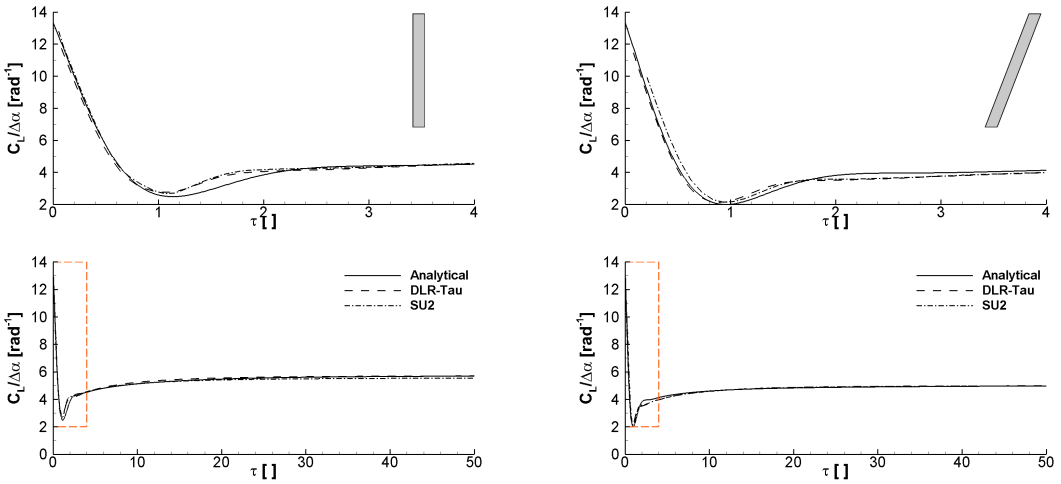

(a) $M = 0.3$, $\Lambda = 0$ deg

(b) $M = 0.3$, $\Lambda = 30$ deg

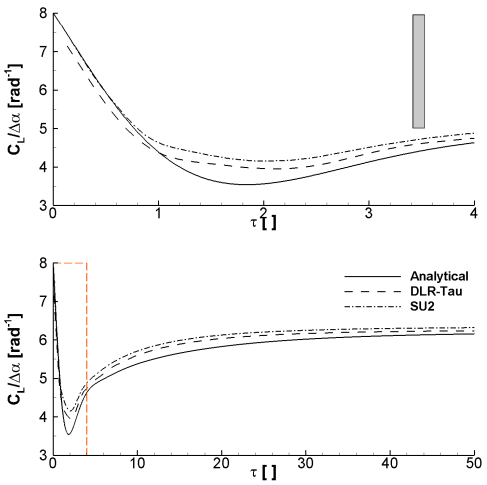

(c) $M = 0.5$, $\Lambda = 0$ deg

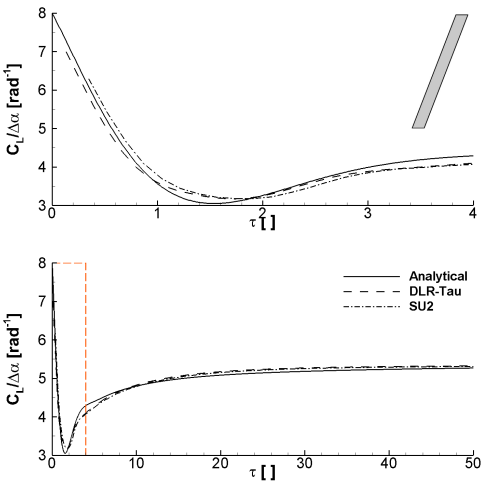

(d) $M = 0.5$, $\Lambda = 30$ deg

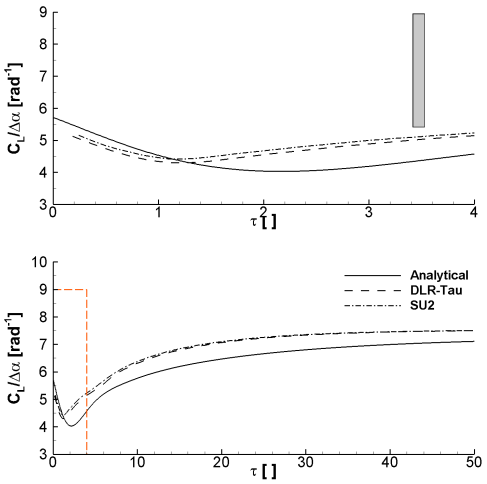

(e) $M = 0.7$, $\Lambda = 0$ deg

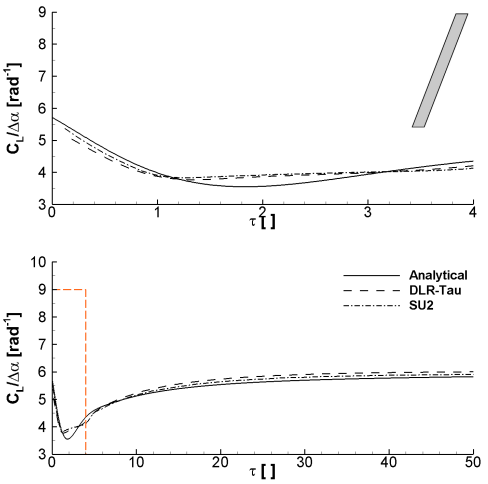

(f) $M = 0.7$, $\Lambda = 30$ deg

Figure 4. Indicial response of lift coefficient to a step change in angle of attack ($\Delta\alpha = 1.0$ deg) for the $AR = 20$ wing; figures on the left are for $\Lambda = 0$ deg, those on the right for $\Lambda = 30$ deg

application of the indicial response allowing the error to be propagated through some intermediate steps. For the significance to aircraft stability and control,[41,42] the quantification of the error is carried out for the prediction of dynamic derivatives.

In this work, the estimation of dynamic derivatives is obtained by imposing a sinusoidal motion around the pitch axis, which is perpendicular to the incoming flow and located at one quarter of the root chord from the leading edge. The harmonic motion in pitch is defined by the relation:

$$\Delta\alpha\,(\tau) \;=\; \alpha_A\,\sin\left(2\,k\,\tau\right) \tag{16}$$

where the amplitude is $\alpha_A = 1$ deg and the reduced frequency is $k = 0.08$. Without resorting to additional (expensive) simulations in the time[41] or frequency domain,[42] dynamic derivatives are efficiently (at no extra costs) predicted using the available indicial responses. The following procedure is applied. First, the lift response to a harmonic motion in pitch is computed using the convolution integral for each indicial response (analytical, `DLR-Tau` and `SU2`). One example is shown in Figure 5(a) for the periodic responses, after the initial transients were removed, at $M = 0.3$ for the $AR = 8$, $\Lambda = 0$ deg wing. Then, one of the methods detailed in Ref.[42] is employed to calculate the dynamic derivatives at the reduced frequency of the forced sinusoidal motion. Herein, emphasis is placed on the prediction of the lift damping coefficient, which consists of two aerodynamic derivatives lumped together: $C_{L_q} + C_{L_{\dot\alpha}}$.

The lift coefficient damping is shown in Figure 5(b) for all test cases. The four wing configurations are reported along the horizontal axis, with the convention described in Table 4. In the figure, analytical predictions are indicated by filled symbols, and the scatter between CFD–based indicial responses is indicated by error bars. The comparisons evince the good general predictive capability of the analytical approach, but some further comments are worth mentioning.

Table 4. Convention to denote wing configurations as labelled in Figure 5(b)

Case	**Wing Configuration**	
Number#	AR	Λ [deg]
1	8	0
2	20	0
3	8	30
4	20	30

The first consideration is that the analytical approach captures the impact of wing planform on the damping coefficient. In particular, increasing the aspect ratio, for a fixed sweep angle, results in a larger damping coefficient, as apparent from the trends that we observe

between the first and the second wing configuration, and between the third and the fourth configuration. The physical reason for this reflects the increased wetted area which generates the damping contribution. Conversely, for a fixed aspect ratio, increasing the sweep angle reduces slightly the damping coefficient value, as revealed by the trends between the first and the third wing configuration, and between the second and the fourth configuration. It seems plausible that this is related to the reduction of the effective angle of attack for a swept–back wing, compared to an unswept case, due the offset between the local aerofoil section and the flow direction, which in turn reduces the lift hysteresis loop.

The scatter in dynamic derivatives, which are computed from CFD–based indicial responses, reflects the associated reliability or uncertainty in the usage of current state–of–the–art CFD solvers for unsteady analyses. The aerodynamic uncertainty in the estimation of dynamic derivatives is relatively large, in specific, when confronted with: i) the background tests performed to minimise the effects of the spatial and temporal resolution, as documented in Section A; and ii) the benign conditions of attached flow (linear steady, linear unsteady) herein considered. It is therefore encouraging to ascertain from Figure 5(b) that the uncertainty associated with the analytical predictions is equivalent to that arising when different CFD solvers are used and compared. The computational cost of the analytical predictions is, however, negligible compared to that needed by the numerical predictions. For reference, SU2 results were computed in about 200 CPU hours.

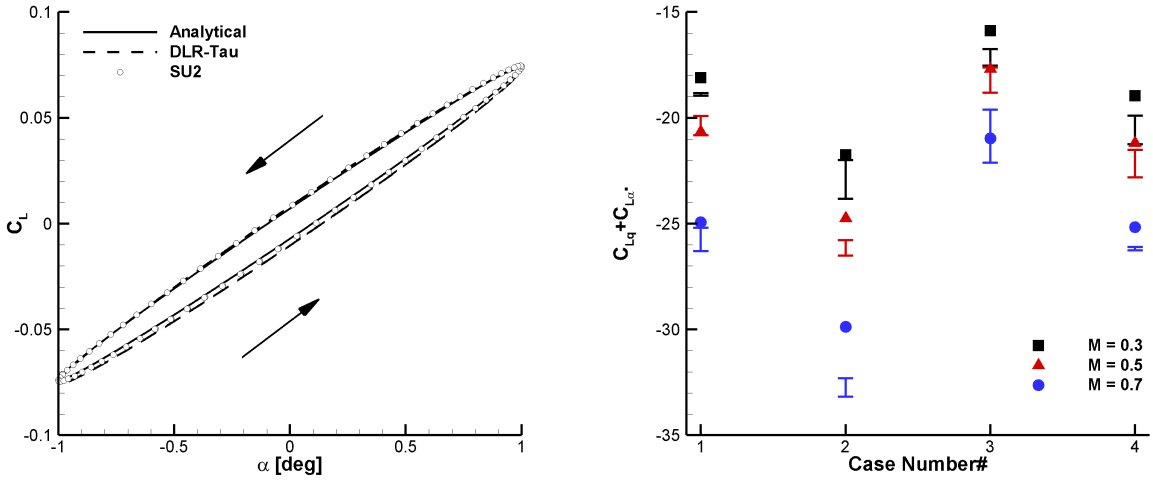

(a) Case Number 1

(b) Lift coefficient damping

Figure 5. In (a), lift response to harmonic motion in pitch ($\alpha_A = 1$ deg, $k = 0.08$, $M = 0.3$) for $AR = 8$, $\Lambda = 0$ deg wing; in (b), lift coefficient damping: filled symbols indicate analytical predictions, error bars the scatter between CFD data

The procedure to obtained dynamic derivatives from the CFD–based indicial responses

is equivalent to that based on the linear frequency domain.[42] Both approaches exploit the assumption of linearity around a (nonlinear) steady state solution. Therefore, conclusions drawn from Figure 5(b) are independent of the particular (indicial) approach used in this study and confirm the general predictive capability of the analytical approach.

D. Indicial Response To Sharp–edge Gust

To the authors' best knowledge, the open literature on the calculation of the indicial response due to a sharp–edge gust is extremely scarce for a three–dimensional wing geometry. In this context, the work reported in this paper provides a thorough study that expands the available background knowledge on indicial functions due to gust for a number of three–dimensional wings. This may be considered the first study in the area, combining analytical and computational techniques. Figures 6 and 7 show the results for all test cases, where the analytical responses use $n_G = 4$ and $m_G = 2$ terms. In particular, the indicial responses of the lift coefficient to a sharp–edge gust for the unswept wing cases ($\Lambda = 0$ deg) are shown in Figure 6, and those for the swept wing cases ($\Lambda = 30$ deg) in Figure 7.

To begin with, the lift built–up for the unswept wing cases reveal a strong similarity between the $AR = 8$ and 20 wings. Small deviations are found between the three aerodynamic sources, but generally the overall agreement is satisfactory. For small times, spurious oscillations appear in the solution obtained using the `DLR-Tau` code. This is not unexpected, as already observed and discussed in the literature.[11] However, it is unexpected that the numerical artefact is solver–dependent, and that `SU2` predicts a smooth gust/wing interaction.

For the swept wing cases, Figure 7 reveals an excellent agreement of the analytical predictions with the computational data. The gradual penetration of the gust front over the wing surface introduces a delay in the lift built–up. Observe that the zoomed area, shown in the upper image of each figure, is for $0 < \tau < 15$, three times larger than the corresponding zoomed area for the unswept case in Figure 6. The resulting gust/wing interaction occurs at a lower rate than for the unswept wing case, but no spurious oscillations were produced by either CFD codes. The reason for this may be attributed to the misalignment between the gust front and the grid elements of the wing surface that develop parallel to the wing leading edge.

E. Error Quantification in Response To Discrete Gust

The one–minus–cosine family of gusts is prescribed by certification authorities for structural sizing of aircraft components. Here, we consider the corresponding aerodynamic problem by neglecting the structural side of the coupled problem. This is justified because an assessment of the recent analytical development is needed in the first place.

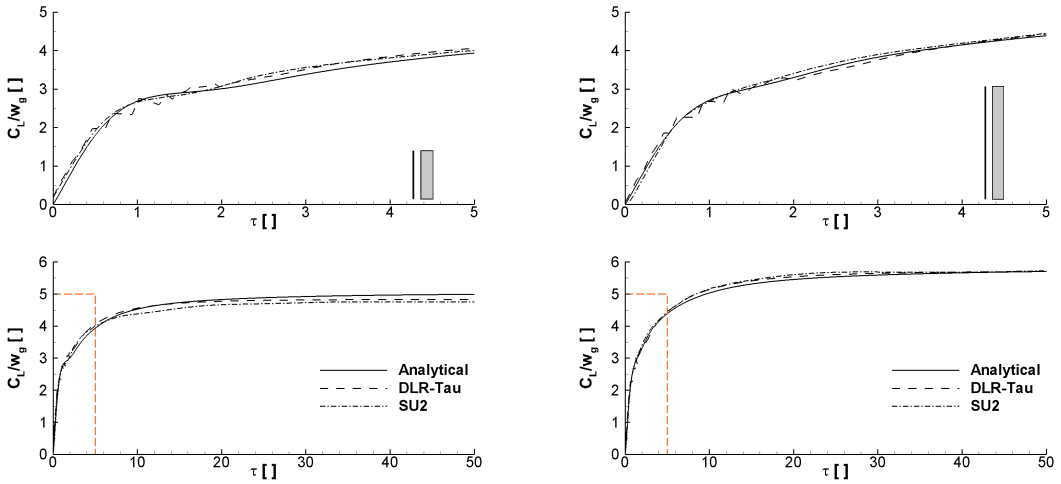

(a) $M = 0.3$, $AR = 8$

(b) $M = 0.3$, $AR = 20$

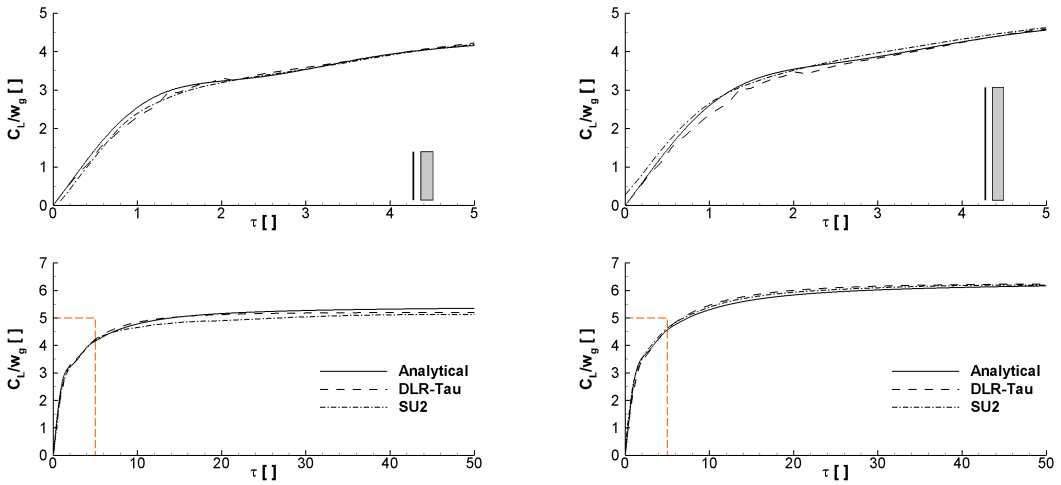

(c) $M = 0.5$, $AR = 8$

(d) $M = 0.5$, $AR = 20$

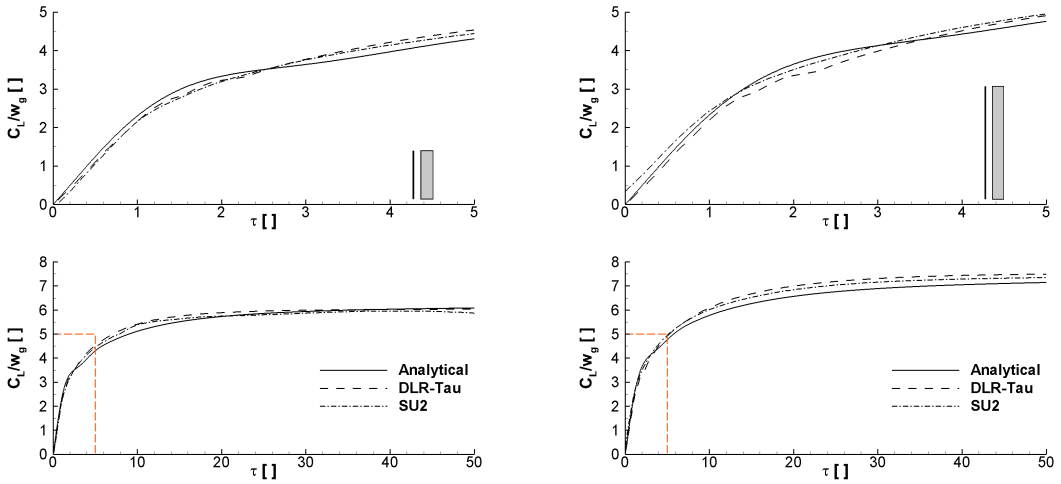

(e) $M = 0.7$, $AR = 8$

(f) $M = 0.7$, $AR = 20$

Figure 6. Indicial response of lift coefficient to a sharp–edge gust for the $\Lambda = 0$ deg wing; figures on the left are for $AR = 8$, those on the right for $AR = 20$

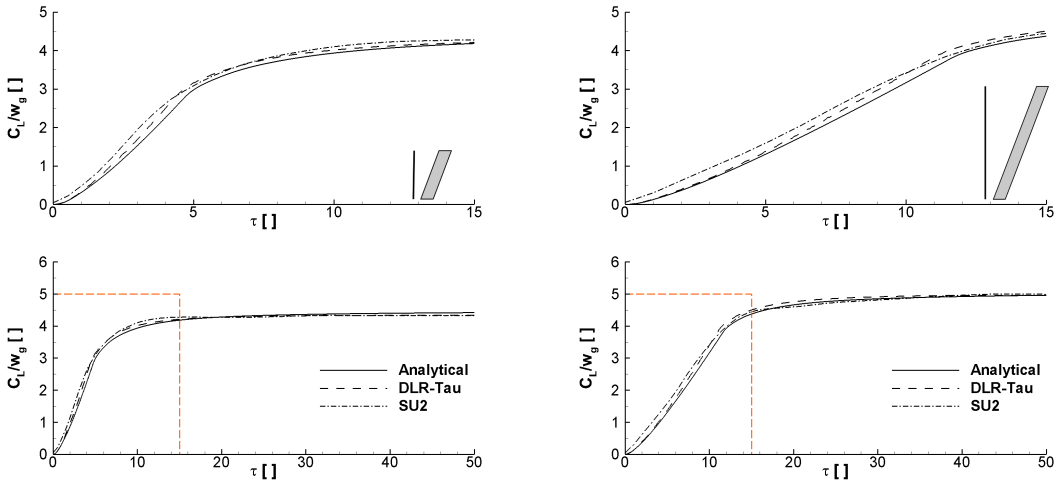

(a) $M = 0.3$, $AR = 8$ (b) $M = 0.3$, $AR = 20$

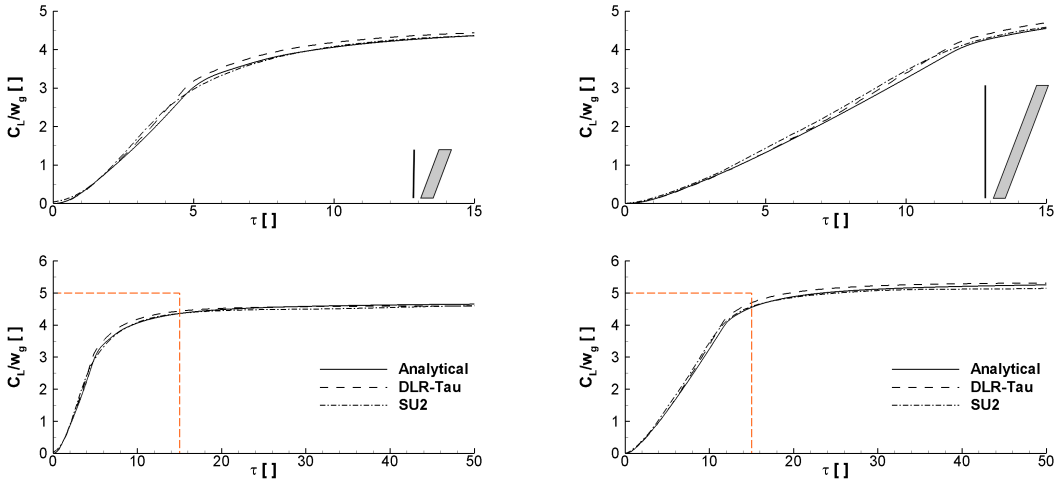

(c) $M = 0.5$, $AR = 8$ (d) $M = 0.5$, $AR = 20$

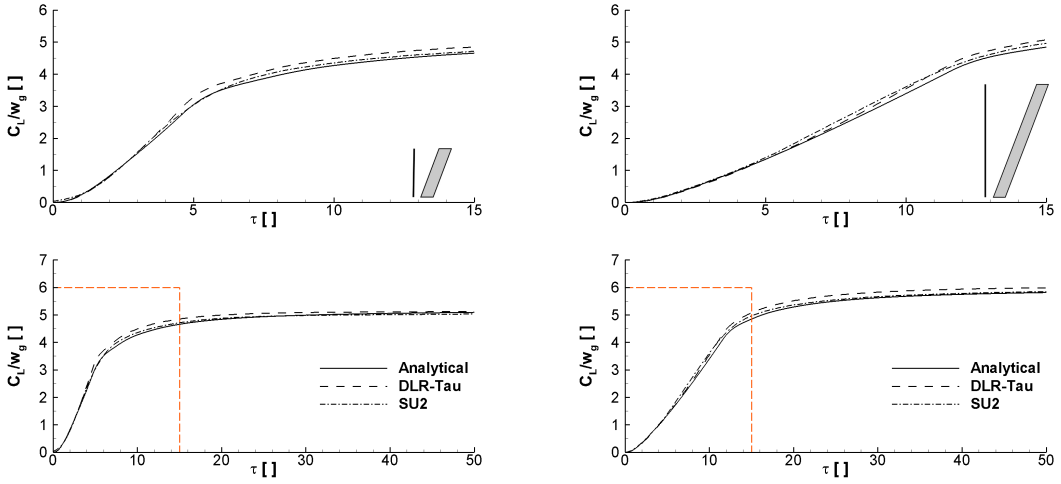

(e) $M = 0.7$, $AR = 8$ (f) $M = 0.7$, $AR = 20$

Figure 7. Indicial response of lift coefficient to a sharp–edge gust with front perpendicular to freestream speed for the $\Lambda = 30$ deg wing; figures on the left are for $AR = 8$, those on the right for $AR = 20$

The nondimensional vertical velocity of a one–minus–cosine gust is modelled as:

$$w_g(\tau) = \frac{w_{g0}}{2}\left(1 - \cos\left(\frac{2\,\pi\,\tau}{H_g}\right)\right) \tag{17}$$

Herein, the focus is for a gust with $w_{g0} = \pi/180$ and $H_g = 25$. The procedure followed consists of two steps. First, the convolution integral is calculated using the available indicial responses from the three aerodynamic sources (Analytical, `DLR-Tau` and `SU2`). An example is shown in Figure 8(a) for the lift coefficient response obtained for the $AR = 8$ and $\Lambda = 0$ deg wing. The second step is the identification of the maximum lift coefficient value, $C_{L\,\max}$, that corresponds to the peak in the response. The maximum lift coefficient recorded for all test cases is illustrated in Figure 8(b).

The uncertainty in the CFD–based aerodynamic predictions is somewhat similar to the deviation of the analytical results from the computational ones. For the unswept wings (case number 1 and 2), the $C_{L\,\max}$ was found to increase for increasing aspect ratio. This ubiquitous trend is a result of the three–dimensionality of the flow: for the shorter wing, the intensity of the tip vortex is stronger, generating a larger (negative) induced angle of attack that partly reduces the effect of the gust encounter. On the contrary, the flow around the slender wing of $AR = 20$ is more two–dimensional, with the tip vortex affecting a relatively smaller portion of the wing surface.

For the swept wings (case number 3 and 4), the aspect ratio has a negligible influence on the maximum lift coefficient. The reason for this is attributed to the similarity between the gust nondimensional length, $H_g = 25$, and the extent of the $AR = 20$, $\Lambda = 30$ deg wing in the downstream direction, that is $AR\tan(\Lambda) \approx 17$. As the gust moves over the wing surface, some areas of the wing may be contemporarily exposed to the left and right ends of the one–minus–cosine gust where the intensity is small, and an isolate part of the wing surface experiences the peak gust.

Finally, it should be expected that the time at which the lift coefficient response reaches the largest peak is case dependent. In particular, the wing sweep angle delays the occurrence, as readily evident from the indicial responses of Section D.

V. Conclusions

Indicial aerodynamics, whether in a linear or nonlinear flavour, remains a convenient modelling technique in light of increased manoeuvre capabilities and expanded flight envelope of modern aircraft. However, the derivation of indicial aerodynamics often relies on either strong limiting assumptions, such as thin aerofoil theory, or on excessing demands in terms

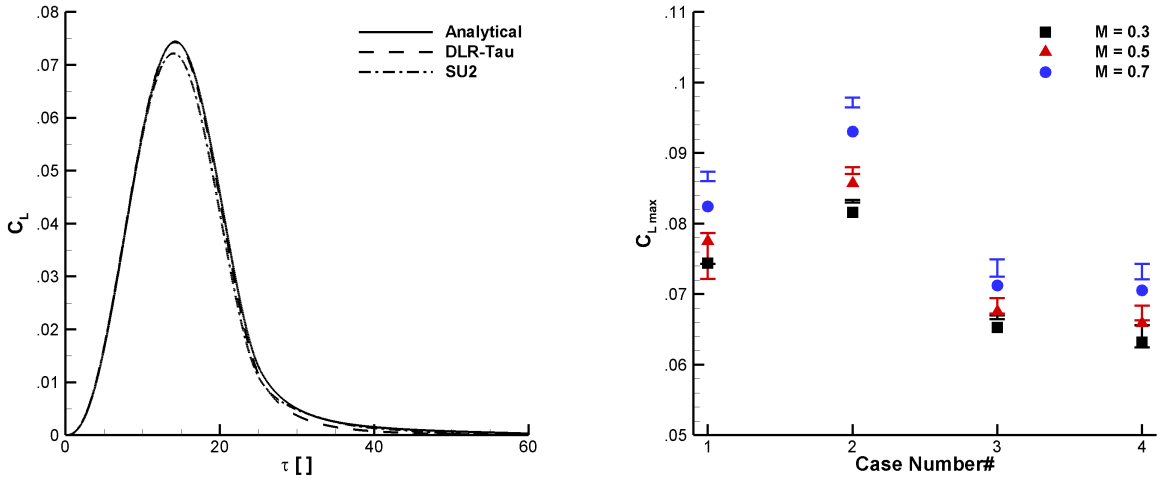

(a) Case Number 1

(b) Maximum lift coefficient

Figure 8. In (a), lift coefficient response to a one–minus–cosine gust ($w_{g0} = \pi/180$, $H_g = 25$, $M = 0.3$) for $AR = 8$, $\Lambda = 0$ deg wing; in (b), maximum lift coefficient: filled symbols indicate analytical predictions, error bars the scatter between CFD data

of computing power and experimental testing. This is the motivation for the present work, which looks at an effective generation of analytical indicial functions.

This work discusses the formulation of an analytical indicial aerodynamics method that extends well–known theories, which are based on the assumption of thin aerofoils, to generic trapezoidal wings of finite span in subsonic flow. Within the chosen analytical method, indicial functions are expanded in series of exponential functions, with coefficients determined by minimising the deviations from the known analytical solutions for incompressible flow. The analytical formulation is then applied to predict the response to a step change in angle of attack and to a sharp–edge gust. The test cases include four wing planforms, with different aspect ratio and sweep angle, at three Mach numbers between 0.3 and 0.7.

Two state–of–the–art computational fluid dynamics solvers (`DLR-Tau` and `SU2`) are used to benchmark analytical predictions for all test cases. The numerical assessments rely on unsteady Reynolds–averaged Navier–Stokes equations with the Spalart–Allmaras turbulence model. Results presented are deemed accurate following spatial and temporal convergence studies.

The first finding of this work is that there is a reasonable agreement between the analytical and computational indicial responses for all test cases. Larger deviations are found within the impulsive/circulatory transition of the responses. Next, the attention was addressed at assessing the impact of the observed deviations in the prediction of dynamic derivatives and the maximum lift coefficient following the encounter with a one–minus–cosine gust. Dynamic

derivatives are computed from available indicial responses to a step change in angle of attack, and the maximum lift coefficient using the indicial responses to a sharp–edge gust. The scatter observed in the computational results was represented with an error bar, representing an equivalent uncertainty in computational aerodynamics. The advantage in doing this is that the deviation of the analytical predictions from the computational results is confronted directly with the scatter or uncertainty arising between the two computational solvers. It is encouraging to ascertain the good predictive capability of the proposed analytical formulation, with results that fall within the scatter or uncertainty in computational values for a good number of test cases. This becomes even more pronounced when balanced against computing costs, with the computational results obtained on high performance computing facilities (200 CPU hours for each unsteady analysis) and after various convergence checks (spatial and temporal).

Appendix on Indicial Lift for Incompressible Flow

A single vortex–ring models the total wing circulation, with both bound and shed vortices parallel to the quarter–chord line and both tip vortices parallel to the freestream. All (lumped) vortices own same intensity, within the simplest implementation of the lifting–line theory. A single control point is then placed at the third–quarter chord of the wing root, where the non–penetration boundary condition is imposed via Kutta–Joukowsky theorem and Biot–Savart law.[43] The shed vortex moves towards infinity at half the reference airspeed from half root–chord behind the control point, thus increasing the wake length and stretching the vortex–ring. After several travelled chords, its influence eventually disappears and the steady lift is asymptotically obtained. The root chord is used as the reference length for the reduced (nondimensional) time τ.

The lift build–up due to a unit step in the angle of attack then reads:[20]

$$\breve{C}_L^{\alpha} = \frac{2\,\pi\,AR_e}{D_B + D_T + D_W}, \qquad AR_e = \left(\frac{1+\lambda}{2}\right) AR \tag{18}$$

where the denominators associated with bound, trailed and shed vortices are:

$$D_B = AR_e \left[\frac{AR_e \sec^2(\Lambda) - \tan(\Lambda)}{\sqrt{\left(AR_e \sec(\Lambda) - \sin(\Lambda)\right)^2 + \cos^2(\Lambda)}} + \tan(\Lambda) \right] \tag{19}$$

$$D_T = \frac{1 - AR_e \tan(\Lambda)}{\sqrt{\left(1 - AR_e \tan(\Lambda)\right)^2 + AR_e^2}} + \frac{1 + AR_e \tan(\Lambda) + \frac{\tau}{2}}{\sqrt{\left(1 + AR_e \tan(\Lambda) + \frac{\tau}{2}\right)^2 + AR_e^2}} \tag{20}$$

$$D_W = \frac{AR_e}{1+\frac{\tau}{2}} \left\{ \frac{AR_e \sec^2(\Lambda) + \left(1+\frac{\tau}{2}\right)\tan(\Lambda)}{\sqrt{\left[AR_e \sec(\Lambda) + \left(1+\frac{\tau}{2}\right)\sin(\Lambda)\right]^2 + \left[\left(1+\frac{\tau}{2}\right)\cos(\Lambda)\right]^2}} - \tan(\Lambda) \right\} \tag{21}$$

leading to $\breve{C}_L^* \equiv \lim_{\tau\to 0} \breve{C}_L^{\alpha}$ and $\bar{C}_L^* \equiv \lim_{\tau\to\infty} \breve{C}_L^{\alpha}$ directly.

Within the "frozen gust" framework,[23] the lift build–up due to a unit sharp–edge gust with perturbation front parallel to the wing leading edge may then be obtained as:

$$\breve{C}_L^G = \left(\frac{K}{W}\right) \breve{C}_L^{\alpha} \tag{22}$$

where K and W are Küssner's[7] and Wagner's[5] functions, respectively, the ratio of which introduces the gust penetration effect.[25] Note that this expression may hold for the case of compressible flow as well;[24] however, all approximation coefficients $\breve{A}_j^G$ and $\breve{B}_j^G$ are then Mach number dependent.[28]

Finally, Figure 9 shows the approximate and original curves considered in this study (see Tables 1 and 2).

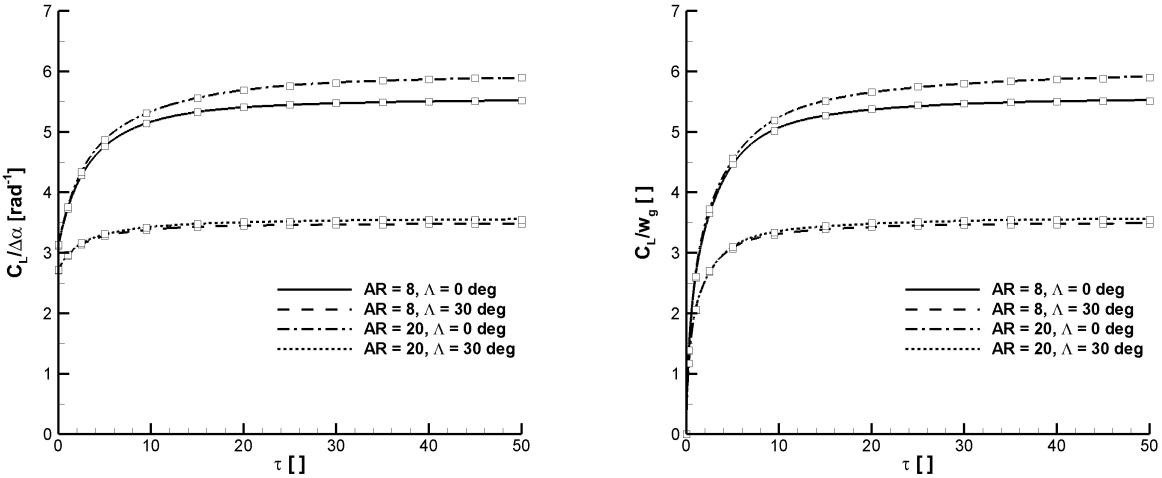

(a) Unit step in the angle of attack

(b) Unit sharp–edge gust

Figure 9. Indicial lift function in incompressible flow: (a) unit step in the angle of attack, (b) unit sharp–edge gust with front parallel to leading edge. Symbols denote the original curves

Acknowledgements

Da Ronch would like to express his sincere appreciation to the Royal Academy of Engineering for funding this research and acknowledges the use of the IRIDIS High Performance Computing Facility, and associated support services at the University of Southampton, in the completion of this work. Righi gratefully acknowledges the computational resources made available by the Swiss National Supercomputing Centre.

Data supporting this study are openly available from the University of Southampton repository at http://dx.doi.org/10.5258/SOTON/xxxxx.

References

[1]Murphy, P. C., Klein, V., and Frink, N. T., "Nonlinear Unsteady Aerodynamic Modeling Using Wind–Tunnel and Computational Data," *Journal of Aircraft*, Vol. Article in Advance, 2016, doi: 10.2514/1.C033881.

[2]Reisenthel, P. H., Bettencourt, M. T., Myatt, J. H., and Grismer, D. S., "A Nonlinear Indicial Prediction Tool For Unsteady Aerodynamic Modeling," AIAA Paper 1998–4350, 1998.

[3]Volterra, V., *Theory of Functionals and of Integral and Integro–Differential Equations*, Dover Publications, Inc., New York, 1959.

[4]Wiener, V., "Response of a Non–Linear Device to Noise," Report No. 129, Radiation Laboratory, MIT, 1942.

[5]Wagner, H., "Üeber die Entstehung des dynamischen Auftriebes von Tragflügeln," *Zeitschrift für Angewandte Mathematik und Mechanik*, Vol. 5, No. 1, 1925, pp. 17–35, doi: 10.1002/zamm.19250050103.

[6]Theodorsen, T., "General Theory of Aerodynamic Instability and the Mechanism of Flutter," NACA 496, 1935.

[7]Küssner, H. G. K., "Stresses Produced in Airplane Wings by Gusts," NASA TM 654, 1932.

[8]Sears, W. R., "Some Aspects of Non–Stationary Airfoil Theory and its Practical Application," *Journal of the Aeronautical Sciences*, Vol. 8, No. 3, 1941, pp. 104–108.

[9]Parameswaran, V. and Baeder, J. D., "Indicial Aerodynamics in Compressible Flow-Direct Computational Fluid Dynamic Calculations," *Journal of Aircraft*, Vol. 34, No. 1, 1997, pp. 131–133.

[10]Ghoreyshi, M., Cummings, R. M., Da Ronch, A., and Badcock, K. J., "Transonic Aerodynamic Loads Modeling of X–31 Aircraft Pitching Motions," *AIAA Journal*, Vol. 51, No. 10, 2013, pp. 2447–2464, doi: 10.2514/1.J052309.

[11]Da Ronch, A., *On the Calculation of Dynamic Derivatives Using Computational Fluid Dynamics*, Ph.d. thesis, School of Engineering, University of Liverpool, U.K., 2012.

[12]Klein, V. and Noderer, K. D., "Modeling of Aircraft Unsteady Aerodynamic Characteristics, Part I: Postulated Models," NASA TM 109120, May 1994.

[13]Klein, V., Murphy, P. C., Curry, T. J., and Brandon, J. M., "Analysis of Wind Tunnel Longitudinal Static and Oscillatory Data of the F–16XL Aircraft," NASA TM 97–206276, December 1997.

[14]Gupta, N. K. and Iliff, K. W., "Identification of Aerodynamic Indicial Functions Using Flight Test Data," AIAA Paper 1982–1375, August 1982.

[15]Myatt, J. H., "Modeling the Rolling 65–Degree DeltaWing with Critical State Encounters," AIAA Paper 1997–3646, August 1997.

[16]Reisenthel, P. H., "Application of Nonlinear Indicial Modeling to the Prediction of a Dynamically Stalling Wing," AIAA Paper 1996–2493, August 1996.

[17]Righi, M., Koch, J., and Berci, M., "Subsonic Indicial Aerodynamics for Unsteady Loads Calculation via Numerical and Analytical Methods: a Preliminary Assessment," *AIAA Aviation Conference*, AIAA–2015–3170, 24–27 June 2015, doi: 10.2514/6.2015-3170.

[18]Gothert, B. H., "Plane and Three-Dimensional Flow at High Subsonic Speeds (Extension of the Prandtl Rule)," NACA TM 1105, 1946.

[19]Pike, E. C., "Manual on Aeroelasticity (Volume II, Chapter VI)," AGARD 578, 1971.

[20]Queijo, M. J., Wells, W. R., and Keskar, D. A., "Approximate indicial lift function for tapered, swept wings in incompressible flow," NASA TP 1241, 1978.

[21]Leishman, J. G., *Principles of Helicopter Aerodynamics*, Cambridge Aerospace Series, Cambridge University Press, 2006.

[22]Jones, R. T., "The Unsteady Lift of a Wing of Finite Aspect Ratio," NASA 681, 1940.

[23]Hoblit, F. M., *Gust Loads on Aircraft: Concepts and Applications*, AIAA Education Series, AIAA, 1998.

[24]Mazelsky, B., "Numerical Determination of Indicial Lift of a Two-Dimensional Sinking Airfoil at Subsonic Mach Numbers from Oscillatory Lift Coefficients with Calculations for Mach number 0.7," NACA TN 2562, 1951.

[25]Chiang, H.-W. D. and Fleeter, S., "Prediction of loaded airfoil unsteady aerodynamic gust response by a locally analytical method," *Mathematical and Computer Modelling*, Vol. 11, 1988, pp. 871–876.

[26]Prandtl, L., "Applications of Modern Hydrodynamics to Aeronautics," NACA TR 116, 1921.

[27]Wieseman, C. D., "Methodology for Matching Experimental and Computational Aerodynamic Data," NACA TM 100592, 1988.

[28]Berci, M. and Righi, M., "An enhanced analytical method for the subsonic indicial lift of two–dimensional aerofoils – with numerical cross–validation," *Aerospace Science and Technology*, Vol. 67, 2017, pp. 354–365.

[29]Bendiksen, O., "Review of unsteady transonic aerodynamics: Theory and applications," *Progress in Aerospace Sciences*, Vol. 47, 2011, pp. 135–167.

[30]Sears, W. R., "Operational methods in the theory of airfoils in non-uniform motion," *Journal of the Franklin Institute*, Vol. 230, No. 1, 1940, pp. 95–111.

[31]Berci, M., "Optimal Approximations of Indicial Aerodynamics," *1st International Conference on Engineering and Applied Sciences Optimization*, 4–6 June 2014.

[32]Lomax, H., Fuller, F. D., and Sluder, L., "Two– and Three–Dimensional Unsteady Lift Problems in High-Speed Flight," NACA 1077, 1952.

[33]Jameson, A., "Transonic Flow Calculations," MAE Report 1651, Princeton University, 1983.

[34]Palacios, F., Colonno, M. R., Aranake, A. C., Campos, A., Copeland, S. R., Economon, T. D., Lonkar, A. K., Lukaczyk, T. W., Taylor, T. W., and Alonso, J. J., "Stanford University Unstructured (SU2): An open-source integrated computational environment for multi-physics simulation and design," *AIAA Paper*, Vol. 287, 2013, pp. 2013.

[35]Palacios, F., Economon, T. D., Aranake, A. C., Copeland, S. R., Lonkar, A. K., Lukaczyk, T. W., Manosalvas, D. E., Naik, K. R., Padrón, A. S., Tracey, B., et al., "Stanford University Unstructured (SU2): Open-source analysis and design technology for turbulent flows," *AIAA paper*, Vol. 243, 2014, pp. 13–17.

[36]Economon, T. D., Palacios, F., Copeland, S. R., Lukaczyk, T. W., and Alonso, J. J., "SU2: An Open-Source Suite for Multiphysics Simulation and Design," *AIAA Journal*, Vol. 54, No. 3, 2015, pp. 828–846.

[37]Roe, P. L., "Approximate Riemann solvers, parameter vectors, and difference schemes," *Journal of computational physics*, Vol. 43, No. 2, 1981, pp. 357–372.

[38]Venkatakrishnan, V., "On the Accuracy of Limiters and Convergence to Steady State Solutions," *AIAA Paper 1993-0880*, 1993.

[39]Venkatesan, C. and Friedmann, P., "New Approach to Finite-State Modeling of Unsteady Aerodynamics," *AIAA Journal*, Vol. 24, No. 12, 1986, pp. 1889–1897.

[40]Nita, M., *Contributions to Aircraft Preliminary Design and Optimization*, Ph.d. thesis, Department of Automotive and Aircraft Engineering, Hamburg University of Applied Sciences, Germany, 2012.

[41]Da Ronch, A., Vallespin, D., Ghoreyshi, M., and Badcock, K. J., "Evaluation of Dynamic Derivatives Using Computational Fluid Dynamics," *AIAA Journal*, Vol. 50, No. 2, 2012, pp. 470–484, doi: 10.2514/1.J051304.

[42]Da Ronch, A., McCracken, A. J., Badcock, K. J., Widhalm, M., and Campobasso, M. S., "Evaluation of Dynamic Derivatives Using Computational Fluid Dynamics," *Journal of Aircraft*, Vol. 50, No. 3, 2013, pp. 694–707, doi: 10.2514/1.C031674.

[43]Katz, J. and Plotkin, A., *Low Speed Aerodynamics*, Cambridge University Press, 2001.